coatings

MDPI

Article

Surface Modification of Carbon Nanotubes in Silicone–Polyurethane for Improved Mechanical and Anticorrosion Properties

Guoqiang Hao [1,†], Xia Li [1,†], Shuchuan Wang [2], Shirong Wang [2], Moonhee Ryu [3,*] and Jingxia Yang [1,2,*]

[1] College of Chemistry and Chemical Engineering, Shanghai University of Engineering Science, LongTeng Road 333, Shanghai 201620, China
[2] T&H Chemicals Co., Ltd., Tangxi Industrial Zone, Quanzhou 362011, China
[3] Division of Biotechnology, College of Environmental and Bioresource Sciences, Chonbuk National University, Iksan 570-752, Republic of Korea
* Correspondence: ryumh@jbnu.ac.kr (M.R.); yjx09tj@foxmail.com (J.Y.)
† These authors contributed equally to this work.

Abstract: Carbon nanotubes (CNT) were dispersed into homemade silicone–polyurethane (SPU) resin in order to enhance their mechanical and anticorrosion ability. Before mixing with SPU, CNT were modified by four different approaches to improve their dispersion in SPU, and the surface of CNT were covered by SiO_2–TiO_2 nanoparticles, -NH_2 groups, epoxy groups or isocyanate groups, respectively. The structures of the modified CNTs were checked by XRD, FTIR, and SEM. After being dispersed in SPU to form a composite coating, the one with SiO_2–TiO_2 nanoparticles modified CNT exhibited the best mechanical properties and chemical resistance (low water absorption), and its corrosion current density (i_{corr}) was only 9.246×10^{-9} A cm^2, which is four orders of magnitude lower than the i_{corr} value of the coating with unmodified CNT (1.599×10^{-5} A/cm^2). This may be because the covered SiO_2–TiO_2 nanoparticle increased the roughness of the CNT surface, which can improve their dispersion in SPU resin.

Keywords: carbon nanotube; silicone–polyurethane; coating; anticorrosion; mechanical property

check for updates

Citation: Hao, G.; Li, X.; Wang, S.; Wang, S.; Ryu, M.; Yang, J. Surface Modification of Carbon Nanotubes in Silicone–Polyurethane for Improved Mechanical and Anticorrosion Properties. *Coatings* **2023**, *13*, 634. https://doi.org/10.3390/coatings13030634

Academic Editor: Stefano Caporali

Received: 31 January 2023
Revised: 4 March 2023
Accepted: 13 March 2023
Published: 17 March 2023

Copyright: © 2023 by the authors. Licensee MDPI, Basel, Switzerland. This article is an open access article distributed under the terms and conditions of the Creative Commons Attribution (CC BY) license (https://creativecommons.org/licenses/by/4.0/).

1. Introduction

Polyurethane (PU) is a multifunctional polymer material with good tensile strength, flexibility, elasticity, resistance to chemical resistance and excellent substrate adhesion; thus, it has a wide range of applications in adhesives, coatings, foam, film, bionic materials and other fields [1–4]. Nevertheless, the disadvantages of PU materials still have limitations for their application, such as poor thermal capability, poor weather ability, and flammability. The silicone modified polyurethane (SPU) can bring the excellent advantages of silicone into the system to enhance PU resin's weather ability, flexibility and water repellency [5–7]. Moreover, in order to endow the PU-based material with additional functions, inorganic nanomaterials are usually selected to form composites with PU, such as carbon nanotubes, graphene or TiO_2 nanoparticles [8–10]. By adding a small part of inorganic nanomaterials, PU performance, such as the anticorrosion and mechanical strength, can be significantly improved [11–14].

Multi-walled carbon nanotube (CNT) is a kind of famous nanofillers for polymers. CNT have excellent properties, such as high electrical conductivity, thermal conductivity and chemical stability [15–17]. Through the formation of hydrogen bonds or strong van der Waals force between PU groups and CNT, different properties can be provided for PU composites [18]. However, the high specific surface area and high surface energy of CNT tend to agglomerate, limiting the performance efficiency of CNT in the PU matrix [19]. To overcome this bottleneck, many approaches have been adopted to improve the arrangement

and dispersion of CNTs, e.g., by in-situ polymerization [20], surface modifications [21] or chemical functionalization [22]. The previous literature has shown that CNTs with these treatments can realize excellent performance when combined with PU. Among the above treatment approaches, surface modification is one of the most effective methods, which can be achieved through a variety of ways, such as surface amination [23–25], carboxylation, silylation and carbonylation [26–28]. In addition, different surface modifications of CNTs can bring different effects to the composites. He et al. modified Fe_2O_3-CNTs hybrid materials with a silane coupling agent (KH560, with an epoxy group), and the prepared Fe_2O_3-CNTs/epoxy resin composite coatings exhibited enhanced mechanical properties and corrosion resistance [14]. Li et al. functionalized hydroxylated CNTs with 3-aminopropyltriethoxysilane via a silylation reaction, and silanes were covalently attached to the surface of CNTs. The modified CNTs showed better dispersion and strong interfacial adhesion to the PU matrix, improving the elongation, hydrophobicity and electrical conductivity of the PU material [29,30]. Although the modification of carbon nanotube has been proven to have positive effects in PU composites, there were normally only one or two modifications for CNTs in each PU system. Besides, research seldom focuses on the effect of CNT in the SPU system. As the properties of the SPU system are somehow different from the PU resin, it is meaningful to figure out the effects of different CNT modification approaches in the SPU system, which may provide the efficiency profiles of surface modification for CNTs application.

In this work, commercial carboxylated multi-walled carbon nanotubes (CNT) were adopted, and different surface modifications of CNT were carried out to check their influences on the performance of the SPU substrate. CNT was modified with amino groups, epoxy groups, isocyanate groups and SiO_2–TiO_2 nanoparticles and further dispersed in homemade silicone modified PU (SPU). The structure of the modified CNT was investigated by FTIR, XRD and SEM, and the mechanical properties and corrosion resistance of the composited CNT-SPU coatings were probed. Possible reasons for the different behaviors of those SPUs with modified CNT were analyzed, and corresponding mechanisms were proposed.

2. Experimental Section

2.1. Materials

4,4′-dicyclohexylmethane diisocyanate (HMDI, >98%) was purchased from Wanhua Chemical Co., Ltd. (Yantai, China); 1,2-epoxybutane (AR), γ-aminopropyl trimethoxysilane (KH540, AR), γ-glycidyl ether oxypropyl trimethoxysilane (KH560, AR), tetraethyl silicate (AR), tetrabutyl titanate (AR) and butyl acetate (ACS) were purchased from Aladdin Reagent Co. (Shanghai, China); Amino Silicone Oil (AS, Industrial grade) purchased from Wanhua Chemical Co. (Yantai, China); Carboxylated multi-walled carbon nanotubes (CNT, >98%) was purchased from CAS Chengdu Co., Ltd. (Chengdu, China); Tianmen Polyurea Resin (1420, Industrial Grade) was purchased from Bayer China (Shanghai, China).

2.2. Preparation of SPU

Home-made silicone modified PU (SPU) was adopted as resin. Amino silicone oil (AS) was modified with 1,2-epoxybutane and further reacted with HMDI to form SPU polymer, as shown in Figure 1.

(1) Preparation of polyols

9.24 g, 1,2-epoxybutane was mixed with 60 g of butyl acetate, and the mixture was added to an appropriate amount of 4A molecular sieve for dehydration and set at room temperature for 10 h. After dehydration, the epoxide solution was poured into a four-necked flask and heated to 55 °C. 100 g of amino silicone oil and 27 g of butyl acetate were added dropwise using a constant pressure funnel, and the reaction was completed at 55 °C for 8 h. The magnetic stirrer was kept at a constant speed throughout the reaction, and the prepared polyol polymer was cooled and set aside. All reactions were carried out under N_2 protection.

(2) Synthesis of prepolymers

HMDI (2.02 g) and butyl acetate (65 g) were added in a three-necked flask with a magnetic stirrer and a thermostat, and the above polyol polymer (20 g) was added dropwise at 0 °C. After the dropwise addition, the reaction was completed for 5 h, and the prepolymer was obtained.

(3) Synthesis of SPU

The 1420 curing agent was added to the prepolymer in the molar ratio HDMI:1420 curing agent = 1:1, left at room temperature for 10 h and then poured into the PTFE mold (20 × 25 × 0.5 cm) and cured at room temperature for 12 h before a complete film could be obtained.

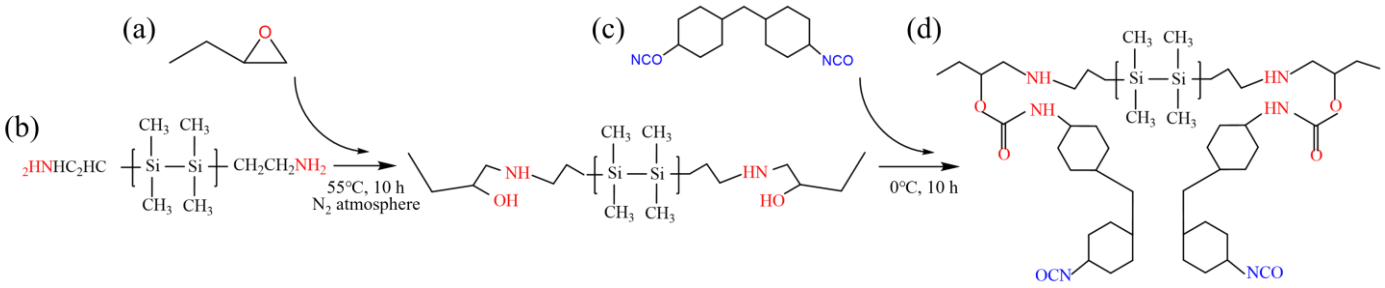


Figure 1. Synthesis of SPU, (**a**) 1,2-epoxybutane; (**b**) amino silicone oil; (**c**) HMDI; (**d**) SPU.

2.3. Modified CNT in SPU Film

Reflux processing was utilized for grafting different functional components on the CNT surface [24]. The modified CNT was mixed with SPU starting materials to prepare composite coatings, as detailed in Figure 2.

(1) Preparation of ***CNT_{MO}-SPU***

Based on previous works [31,32], CNT (0.4 g) were ultrasonically dispersed in a mixture of deionized H_2O (100 mL) and ethanol (EtOH) (20 mL) for 30 min to obtain a homogeneous suspension. Tetraethyl orthosilicate (0.4 g) and tetrabutyl orthotitanate (0.68 g) were dissolved in EtOH (80 mL) and added into the CNT suspension and stirred at room temperature for 8 h, and a thin SiO_2–TiO_2 nanoparticle covered on the surface of CNT. Then the SiO_2–TiO_2 nanoparticles modified CNT solids were collected, washed three times with EtOH and dried in vacuum at 80 °C for 12 h to obtain ***CNT_{MO}***.

CNT_{MO} material (0.025 wt% of SPU) was dispersed into the SPU starting materials, and a similar procedure was carried out as pure SPU film preparation (Section 2.2). The final prepared film was named ***CNT_{MO}-SPU***, as shown in Figure 2a.

(2) Preparation of ***CNT_{NH2}-SPU***

CNT surface was modified by NH_2 groups according to the previous literature [14]. Firstly, KH540 (10 mL) was mixed with deionized H_2O (90 mL) and hydrolyzed for 30 min. Then, CNT (0.4 g), H_2O (20 mL) and EtOH (60 mL) were added to the KH540-solution and sonicated for 30 min. The solution was refluxed at 80 °C for 6 h to graft the NH_2 groups on the CNT surface. The NH_2 groups modified CNT solids were collected, washed three times with EtOH and dried in vacuum at 80 °C for 12 h to obtain ***CNT_{NH2}***.

CNT_{NH2} (0.025 wt% of SPU) was added to SPU starting materials, and the final prepared free-standing film was named ***CNT_{NH2}-SPU***, as shown in Figure 2b.

(3) Preparation of ***CNT_{EP}-SPU***

CNT was modified with epoxy groups using KH560 in the same way as the preparation of ***CNT_{NH2}***. ***CNT_{EP}*** (0.025 wt% of SPU) was added to SPU starting materials, and the final prepared free-standing film was named ***CNT_{EP}-SPU***, as shown in Figure 2c.

(4) Preparation of CNT_{NCO}-SPU

CNT surface was modified by isocyanate (NCO) groups according to the previous literature [31]. CNT (0.4 g) was dispersed into DMF (50 mL), and then HMDI (0.4 g) was added. The mixture was stirred and refluxed at 60 °C for 6 h to grow isocyanate groups on the CNT surface. The NCO groups modified CNT solids were collected, washed three times with EtOH and dried in vacuum at 80 °C for 12 h to obtain CNT_{NCO}.

CNT_{NCO} (0.025 wt% of SPU) was added to SPU starting materials, and the final prepared free-standing film was named CNT_{NCO}-SPU, as shown in Figure 2d.

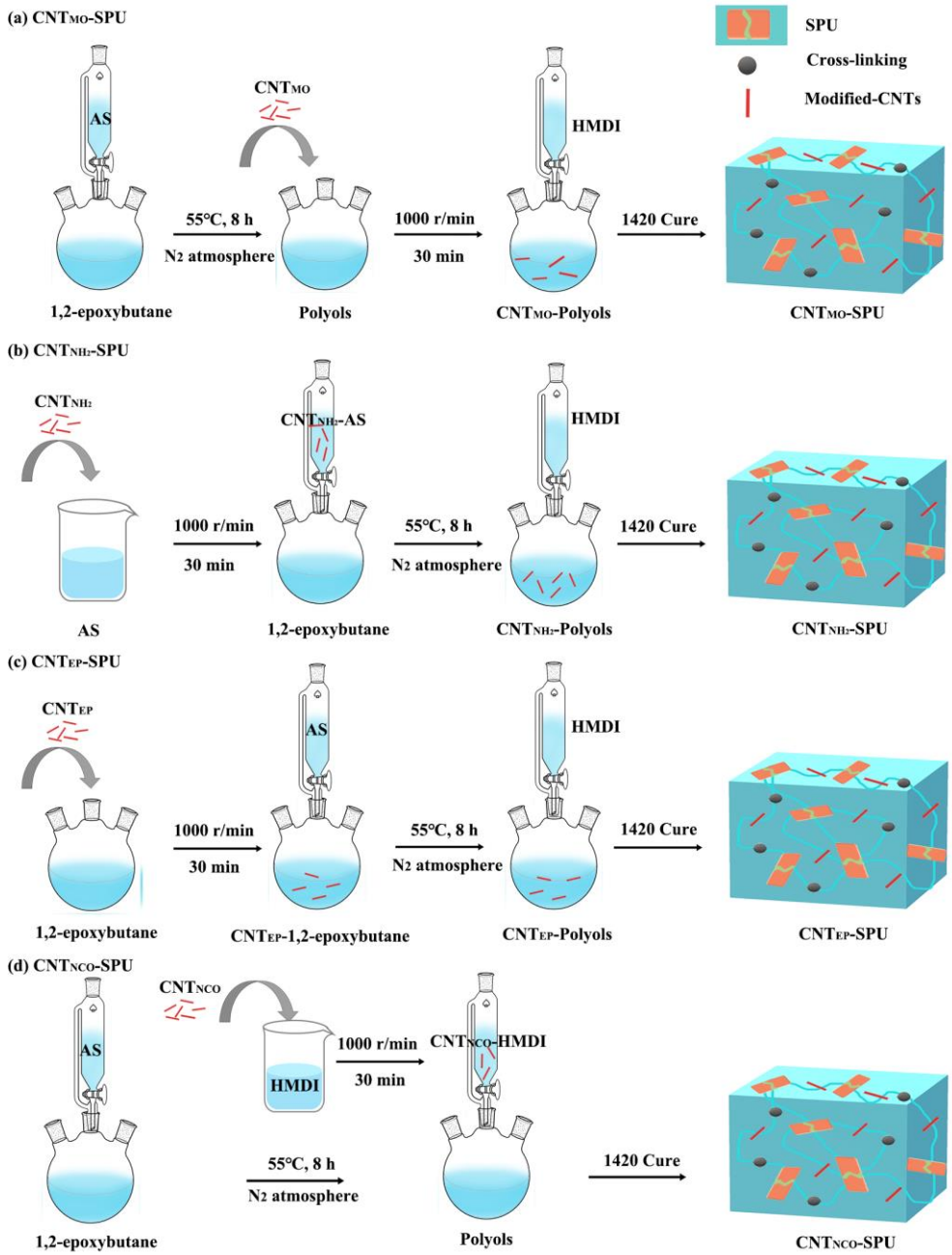


Figure 2. Experimental scheme of modified CNT in SPU. (**a**) preparation of CNT_{MO}-SPU; (**b**) preparation of CNT_{NH2}-SPU; (**c**) preparation of CNT_{EP}-SPU; (**d**) preparation of CNT_{NCO}-SPU.

2.4. Characterization

2.4.1. Structure Characterization

To characterize the functional groups of the CNT, Fourier transforms infrared spectrometer (FTIR, Thermo Fisher Scientific 370, Waltham, MA, USA) was used with a frequency range of 4000–500 cm^{-1}.

The crystallization properties of the samples were analyzed by X-ray diffraction (XRD). The D2-phase, Cu Kα1 line (λ = 1.5406 Å) form Bruker Corporation (Bruker, Billerica, MA, USA) was used, operating at 40 kV/40 mA with 2θ ranging from 10° to 90°.

Scanning electron microscope (SEM) images were obtained by using a Hitachi S–8000 field emission scanning electron microscope (Tokyo, Japan). The cross-section of the sample was scanned at an accelerated voltage of 5 kV, and the sample was quenched in liquid nitrogen before breaking for characterization.

2.4.2. Mechanical Properties of Modified CNT-SPU Films

The mechanical properties of the composite films were investigated according to ISO 37:2005. Five dumbbell samples were tested by CZ–8000 from Zhongzhi Testing Instruments (Shanghai, China), and the tensile rate was 20 mm/min. Each sample was measured at least five times, and the average tensile properties were calculated.

2.4.3. Water and Chemical Resistance Testing of Modified CNT-SPU Films

The water and chemical resistance of the coating were evaluated by the water absorption of the film during storage at room temperature (25 °C) in deionized water, 1 wt% hydrochloric acid and NaOH. The water absorption of the film is determined by measuring its weight immersion for more than 48 h, and the water absorption is calculated according to the following formula:

$$W = \frac{(m_2 - m_1)}{m_1} \times 100\% \quad (1)$$

W—water absorption, wt%; m_1—the weight of the dry film, g; m_2—weight after water absorption, g.

2.4.4. Anticorrosion Performance

For the anticorrosion test, the ***CNT-SPU*** and ***CNT_{MO}-SPU*** composites resin were coated on a tinplate by a wet coating preparation device (Huaguo Precision Instrument Co., Ltd., Guangzhou, China), and the coating thickness was 200 μm. The tinplate was polished with sandpaper before use. The coating was tested after curing at room temperature for one week to ensure that the CNT-SPU composite coatings contact well with the polished tinplate substrate, and the obtained samples were named "***CNT-SPU coating***" and "***CNT_{MO}-SPU coating***", respectively.

Potentiodynamic polarization curves and electrochemical impedance (EIS) tests were performed using a CHI600E electrochemical workstation (Chenhua Instruments, Shanghai, China). The test sample was partially immersed in a 3.5 wt% NaCl solution, and a classical three-electrode working system was adopted. The coated steel plate was used as the working electrode (exposed area of 1 cm^2), the saturated glycolic electrode (SCE) was used as the reference electrode, and a platinum sheet (area of 1 cm^2) was used as the counter electrode. The potentiodynamic polarization curve was scanned at a rate of 0.05 V/s, and the EIS was scanned at a frequency of 10^{-2} to 10^5 Hz. The experimental data were fitted with Zsimpwin software (V3.30).

3. Results and Discussion

3.1. Structure of Modified CNT

Figure 3 illustrates the FTIR spectra for ***CNT***, ***CNT_{MO}***, ***CNT_{NH2}***, ***CNT_{EP}*** and ***CNT_{NCO}***, and the differences in functional groups on the surface of CNT can be observed. The representation of each peak is summarized in Table 1. For pure ***CNT*** (Figure 3a_1), the broad peak at 3445 cm^{-1} is caused by -OH liberation on the CNT surface. The peaks in the

range of 2800 to 3000 cm^{-1} are due to CH_2/CH_3 from the alkyl chain in the precursors, and the peak at 1640 cm^{-1} is caused by the interaction of the skeletal CNT and carboxyl. Besides, the peak in the range of 600 to 700 cm^{-1} is caused by C-S groups from CNT [33], which was generated during the CNT preparation by H_2SO_4 washing. This C-S peak can be observed in all modified CNT samples, indicating C-S bond was not involved in any modification reaction. However, the peak intensity of the C=O group (COOH) at 1640 cm^{-1} reduced heavily after the surface modification, which may be evidence of the successful modification. In the ***CNT$_{MO}$*** FTIR spectrum (Figure 3a$_2$), additional absorption bands related to Si-O-Si (970–1100 cm^{-1}), Si-OH (870 cm^{-1}), Ti-O-Ti (500–800 cm^{-1}), and Ti-O-C (1210 cm^{-1}) vibrations appeared [32,34,35]. These results indicate that the SiO_2 and TiO_2 have successfully formed on CNT. When ***CNT$_{NH2}$*** is concerned (Figure 3a$_3$), the presence of KH540 can be confirmed by the characteristic peaks of -CH_2 and -NH_2 at 2910 cm^{-1} and 3400 cm^{-1} and the peak of C-N at 1120 cm^{-1}. Figure 3a$_4$ shows the FTIR spectrum of ***CNT$_{EP}$***. The characteristic absorption bands of -C-O-C- appeared at 1050 cm^{-1}, suggesting that part of KH560 silane has been linked to the CNT surface. When ***CNT$_{NCO}$*** is checked, its FTIR spectrum (Figure 3a$_5$) has the characteristic absorption peaks of -NCO at 2250 cm^{-1}, indicating the carboxyl group on the surface of CNT reacted with HMDI, and the -NCO group was successfully grafted onto the surface of CNT.

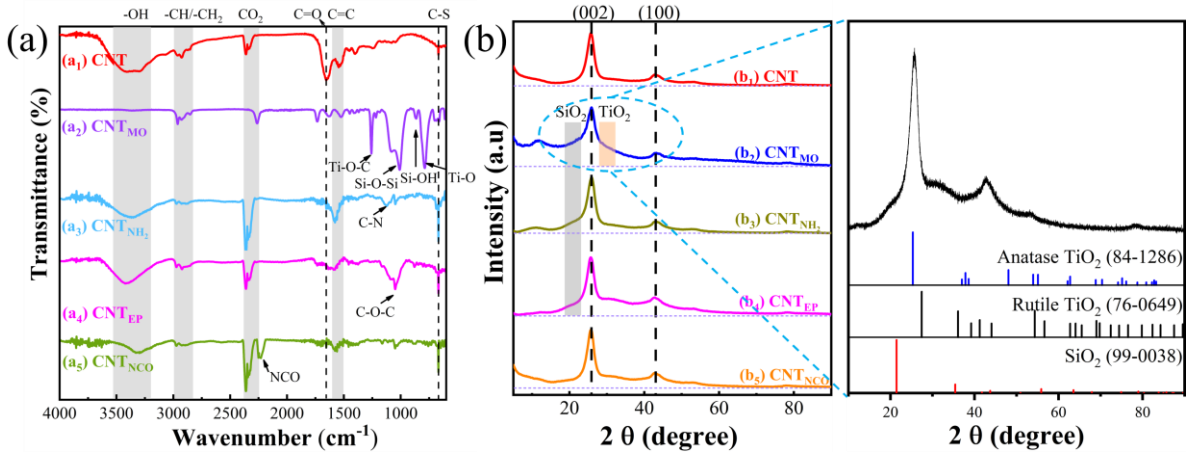


Figure 3. (**a**) FTIR spectra(a) and XRD results (**b**) of pristine and four modified CNT inorganic filler.

Table 1. The representation of each peak.

Wavenumber (cm^{-1})	Functional Group	Characteristic Vibration Mode for
3600–3200	-OH	surface carboxylic, -OH from absorbed H_2O in the air
3400	-NH_2	N-CNT, NH or NH_2
3000–2800	CH_2/CH_3	from alkyl chain
2350	CO_2	CO_2 from the air
2250	-NCO	isocyanate (-N=C=O)
1640	C=O	the skeletal CNT and carboxyl or ketone groups
1580–1530	C=C	hexagonal structure on the pristine CNTs
1210	Ti-O-C	from tetrabutyl titanate
970–1100	Si-O-Si	SiO_2 and silanes
870	Si-OH	silanes
1120	C-N	from KH540
500–800	Ti-O-Ti	TiO_2
663	C-S	CNT

The structural changes of surface-modified CNT were further evaluated by XRD (Figure 3b). For pure ***CNT*** (Figure 3b$_1$), the typical peaks of carbon nanotubes appeared at 2θ = 25.8° and 43.1°, corresponding to (002) and (100) planes, respectively [36]. After various surface modifications (Figure 3b$_2$–b$_5$), the (002) and (100) peaks of CNT can also

be observed, indicating that the crystal structure of the CNT did not change due to group modification. Nevertheless, except for $\boldsymbol{CNT_{NCO}}$ (Figure 3b$_5$), an enhanced shoulder appeared on the left of the (002) peak for the CNT samples modified by SiO_2–TiO_2, KH540 and KH560 (Figure 3b$_2$–b$_4$). This left shoulder of the CNT (002) peak may be caused by amorphous/nanocrystalline SiO_2, as the Si component existed in their modification precursors. Besides, an obvious right shoulder can be found near the (002) peak of the $\boldsymbol{CNT_{MO}}$ XRD spectrum (Figure 3b$_2$), which can be considered as amorphous/nanocrystalline titanium dioxide [37,38]. As the diffraction peaks of rutile TiO_2 is closer to the right shoulder of the CNT (002) peak, and it maybe exists as rutile TiO_2.

According to the preparation procedure and the FTIR&XRD results, Figure 4 shows the surface changes of CNT. In the $\boldsymbol{CNT_{MO}}$ sample (Figure 4a), tetraethyl silicate and tetrabutyl titanate were hydrolyzed and condensed to form SiO_2–TiO_2 nanoparticles on the CNT surface. For $\boldsymbol{CNT_{NH2}}$, $\boldsymbol{CNT_{EP}}$ and $\boldsymbol{CNT_{NCO}}$ (Figure 4b–d), KH540, KH560 and HMDI were used for each, and the siloxy group and -NCO group reacted with the COOH of the CNT surface, so the NH_2, epoxy and NCO group grafted on the CNT surface, respectively.

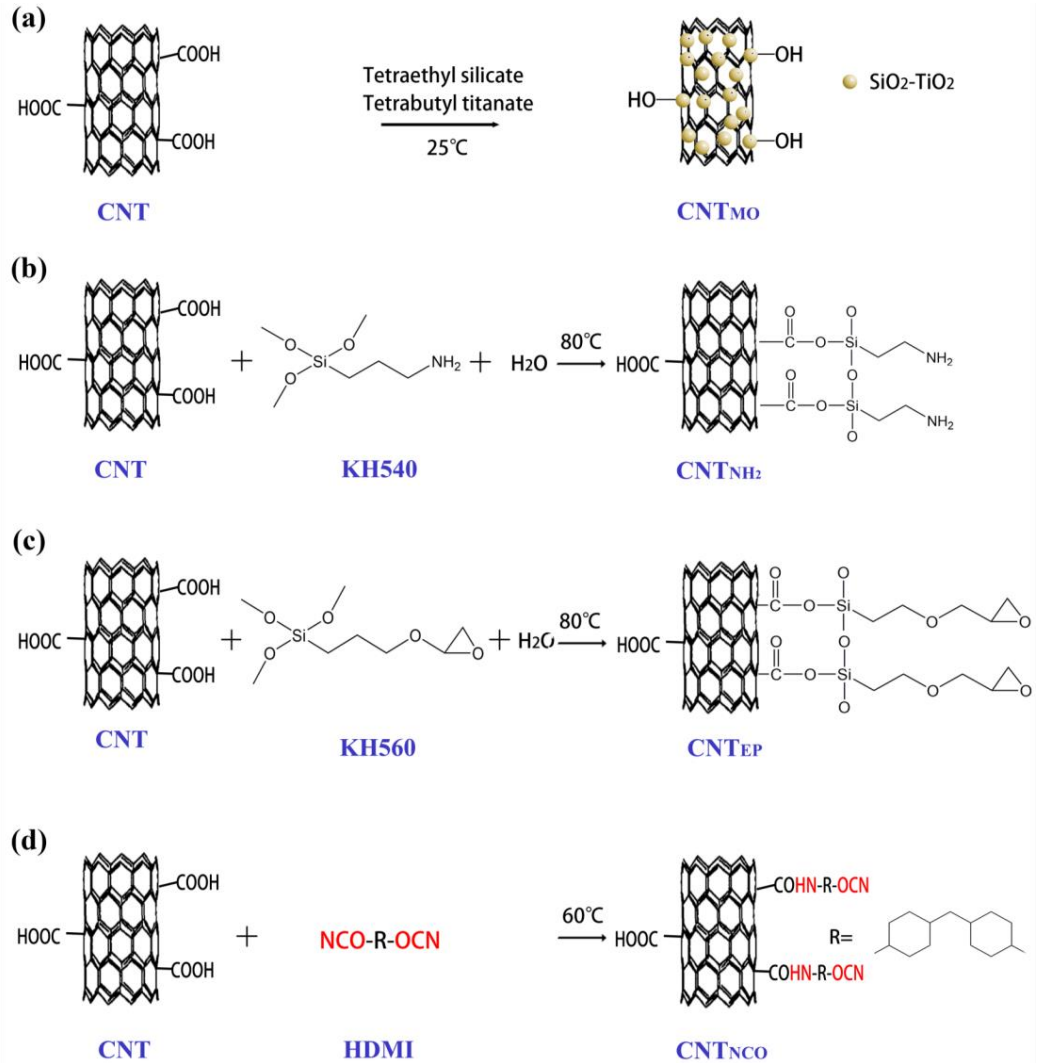


Figure 4. Scheme of surface changes of modified ***CNT***. (**a**) $\boldsymbol{CNT_{MO}}$; (**b**) $\boldsymbol{CNT_{NH2}}$; (**c**) $\boldsymbol{CNT_{EP}}$; (**d**) $\boldsymbol{CNT_{NCO}}$.

The morphologies of CNT before and after modification were studied by SEM (Figure 5a$_1$–e$_1$). The tube wall of pure ***CNT*** (Figure 5a$_1$) is smooth and relatively clean. The $\boldsymbol{CNT_{MO}}$ (Figure 5b$_1$) surface is rough, indicating SiO_2–TiO_2 particles grown on the surface of the tube. According to previous reports, SiO_2 and TiO_2 prefer to stay together without

phase separation [39,40], and the following EDS and elemental mapping (Figure 6c and $c_{1–3}$) confirmed this. ***CNT$_{NH2}$*** (Figure 5c_1) and ***CNT$_{EP}$*** (Figure 5d_1) seem to be covered with a coating on the CNT tube, which may be due to the reaction of the COOH group on the CNT with KH540 and KH560, respectively. The scale-like structure appeared on the surface of ***CNT$_{NCO}$*** (Figure 5e_1), which may be related to the reaction of the COOH group on CNT with NCO in HMDI. The cross-sectional morphologies of unmodified and modified CNT-SPU were checked by SEM (Figure 5a_2–e_2), and no obvious differences can be observed for the CNT-SPU films with different CNT samples, which may be due to the small amount of CNT added. However, the phase separation of ***CNT$_{NCO}$-SPU*** film (Figure 5e_2) becomes serious. This may be due to the additional order of NCO compounds leading to poor polymerization of silicone resin and polyurethane. Nevertheless, for ***CNT*** and ***CNT$_{MO}$***, their dispersion states in solution were characterized by a metallographic microscope (Figure 6), and the dispersion of ***CNT$_{MO}$*** (Figure 6b) is much more homogeneous than that of the unmodified CNT sample (Figure 6a), indicating the surface modification of ***CNT*** can overcome the agglomeration between the CNTs. The microstructure of the ***CNT$_{MO}$*** was analyzed through SEM technology coupled with EDS and elemental mapping. As shown in Figure 6c, it clearly indicates that Ti and Si elements are homogeneously dispersed on ***CNT$_{MO}$***, and this strongly suggests the successful loading of SiO_2–TiO_2 nanoparticles on the CNT.

3.2. Mechanical Properties of SPU Films with Modified CNT

Pure ***CNT*** and various modified CNTs were dispersed in SPU, forming different CNT-SPU composites, and their mechanical properties were checked, as shown in Figure 7. The elongation at break and tensile strength can reflect the toughness and strength of the composite films. The tensile strength and elongation at the break of the ***CNT-SPU*** film were 2.81 MPa and 146%, respectively. After CNT were modified, the tensile strength values of the ***CNT$_{MO}$-SPU*** and ***CNT$_{NH2}$-SPU*** increased by 0.64 MPa and 0.99 MPa, respectively, compared to the unmodified ***CNT-SPU*** composite film, while the tensile strength of the KH560 and NCO modified materials decreased slightly. Only the elongation at the break of the SiO_2–TiO_2 modified elastomer (***CNT$_{MO}$-SPU***) increased, and the elongation at the break of the other three modified composite films decreased. The interfacial strength between inorganic fillers and SPU determines the mechanical properties of the composite elastomer. This change may be because the addition of modified CNT changed the crosslinking degree of SPU. The SiO_2–TiO_2 encapsulation reduced the surface free energy of CNT, and the surface OH groups formed chemical bonds with SPU, which improved the crosslinking of SPU and enhanced the dispersion of CNT [31]. Although both ***CNT$_{NH2}$-SPU*** and ***CNT$_{EP}$-SPU*** were modified by silane coupling agents, due to a small structure of KH540, ***CNT$_{NH2}$*** may have small steric hindrance and good compatibility with the NCO group of SPU, resulting in better mechanical properties than the one with KH560. The ***CNT$_{NCO}$-SPU*** film performance became worse, probably because that part of the NCO groups on the surface of the filler reacted with H_2O and are not connected to the SPU main chain. In addition, the ***CNT$_{NCO}$*** forms a physical fill in it; thus, its mechanical property is not as good as the film covalent bonding with SPU. Nevertheless, when compared with the values in the literature (Table 2), our samples showed not very good mechanical properties, and the value is only comparable with the one using silicone modified waterborne polyurethane (3.47 MPa, 104.47%) [41]. This may be because the silicone component can reduce the tensile strength, as described in the reference [41]. The smaller elongation break indicated that the crosslinking was high in the CNT-SPU samples, which can well prevent water penetration, as shown in the following section.

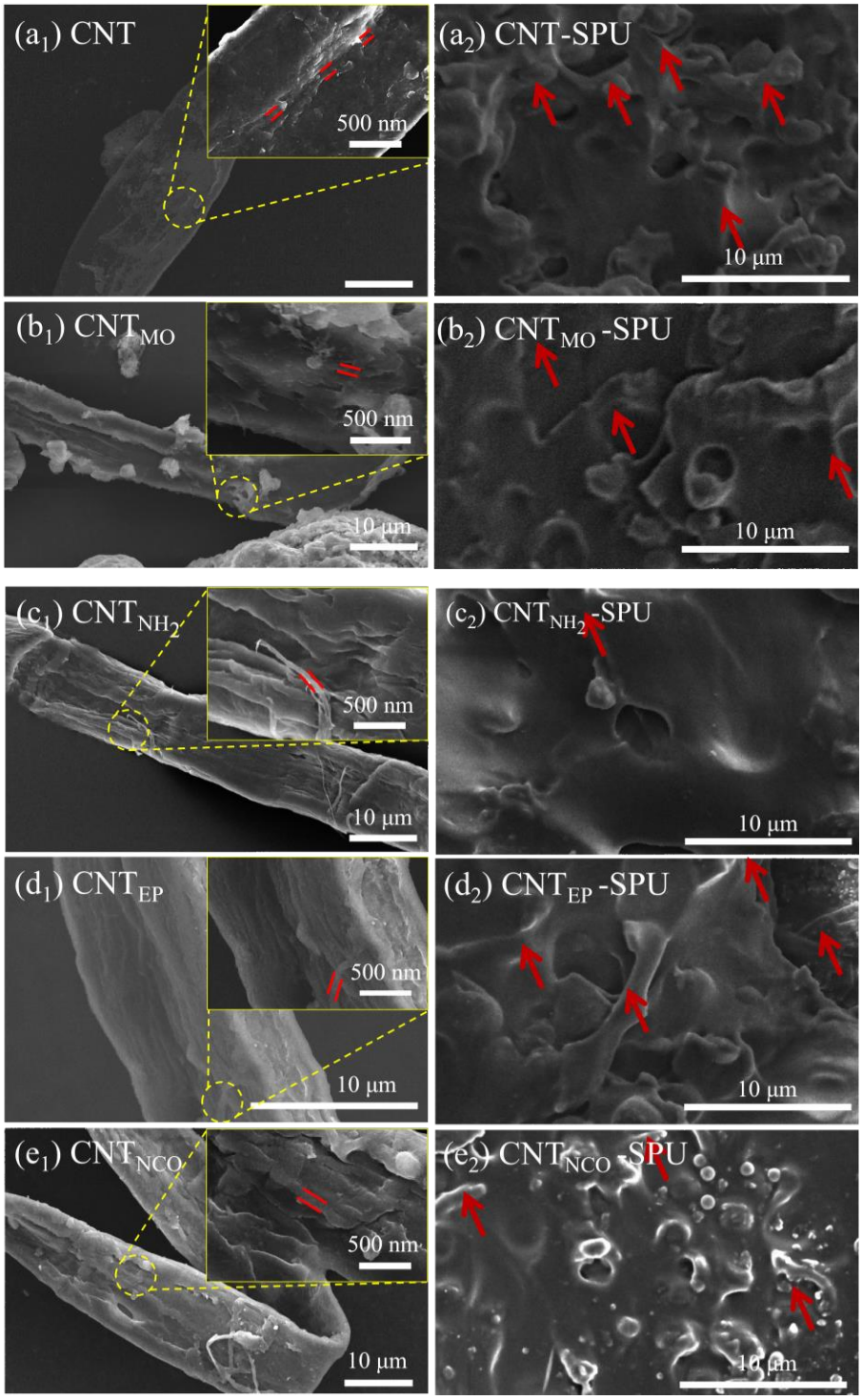


Figure 5. SEM pictures of modified CNT samples ((**a$_1$**–**e$_1$**) Multiple: 2 k, Multiple for insert: 50 k) and the cross-section of various CNT-SPU composite films ((**a$_2$**–**e$_2$**) Multiple: 5 k): (**a$_1$**) ***CNT***, (**b$_1$**) ***CNT$_{MO}$***, (**c$_1$**) ***CNT$_{NH2}$***, (**d$_1$**) ***CNT$_{EP}$***, (**e$_1$**) ***CNT$_{NCO}$***, (**a$_2$**) ***CNT-SPU***, (**b$_2$**) ***CNT$_{MO}$-SPU***, (**c$_2$**) ***CNT$_{NH2}$-SPU***, (**d$_2$**) ***CNT$_{EP}$-SPU***, (**e$_2$**) ***CNT$_{NCO}$-SPU***.

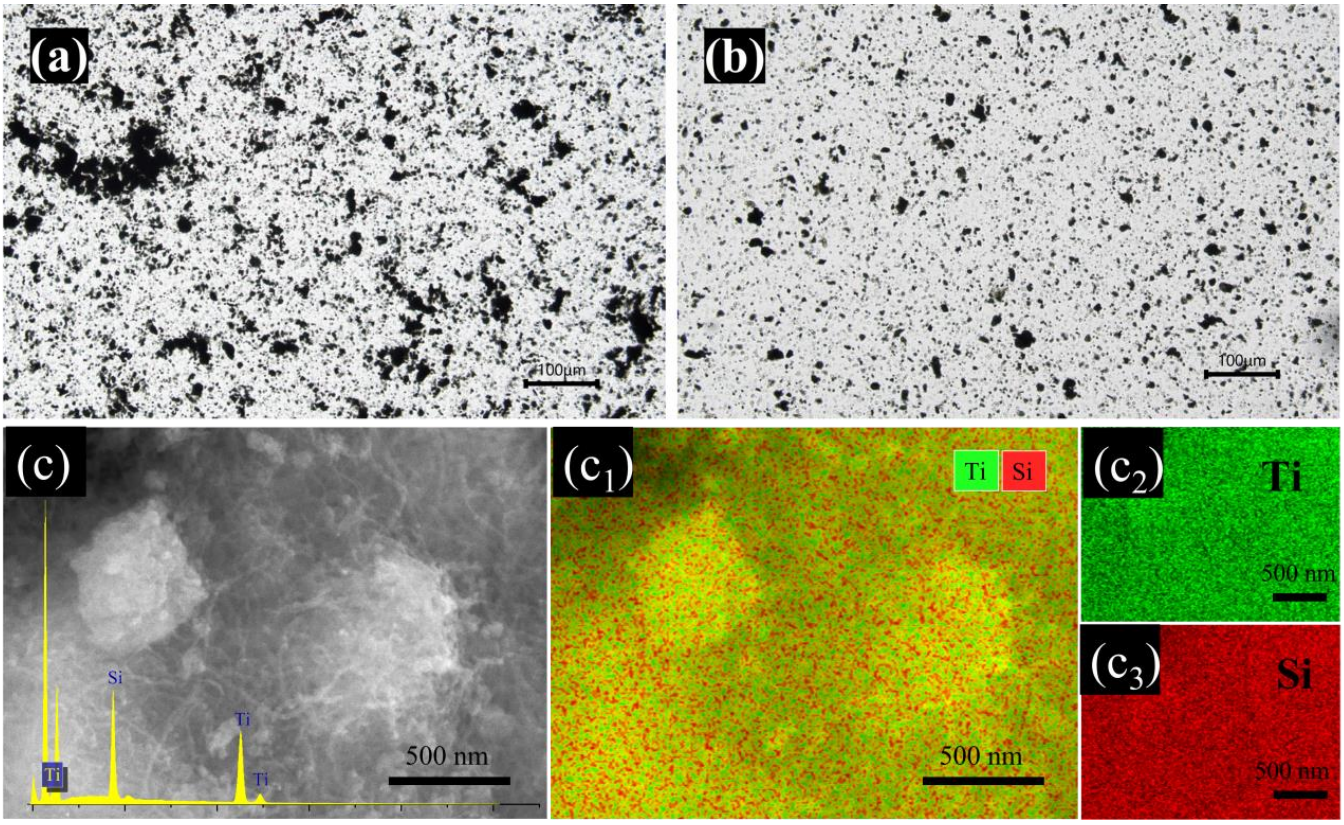


Figure 6. Metallographic microscopic photographs of unmodified ***CNT*** (**a**) and ***CNT$_{MO}$*** (**b**) in SPU resin; EDS (**c**) and elemental mapping of ***CNT$_{MO}$*** (**c$_1$**–**c$_3$**).

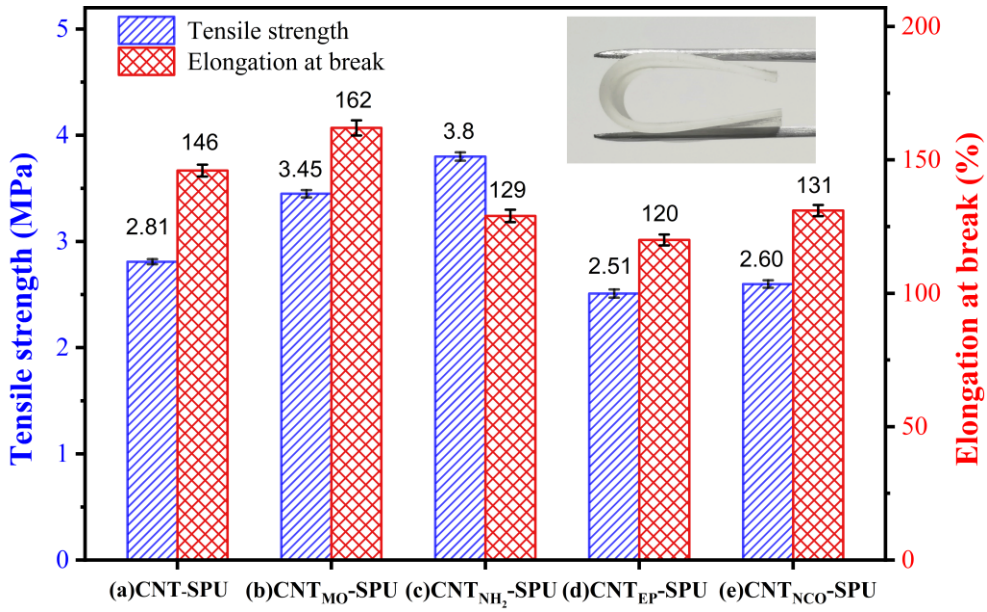


Figure 7. Mechanical properties of CNT-SPU composite free-standing film before and after modification: (**a**) ***CNT-SPU***, (**b**) ***CNT$_{MO}$-SPU***, (**c**) ***CNT$_{NH2}$-SPU***, (**d**) ***CNT$_{EP}$-SPU***, (**e**) ***CNT$_{NCO}$-SPU***. The insert in the upper right corner is the photo of ***CNT$_{MO}$-SPU*** free-standing film.

Table 2. Summary of mechanical properties and water absorption of SPU.

Sample	Tensile Strength (MPa)	Elongation Break (%)	Water Absorption (%)	Reference
CNT_{MO}-SPU	3.45	162	0.360 ± 0.053	This work
WPU-Si	3.47 ± 0.52	104.47 ± 9.21	12.58 ± 0.81	Qian, Y. et al. [41]
0.1 wt% CNT/PU–silicone composite	12.7 ± 2	710 ± 40	/	Tijing, L. D. et al. [42]
P1-60	/	/	0.90	Kurańska, M. et al. [43]
WPU-3	22.4 ± 0.5	781.1 ± 13	7.6	Zhang, X. J. et al. [44]
SPU-4	7.0	366.5	0.50	Xu, S. et al. [45]
MD	72.5 ± 3.5	3.6 ± 0.3	/	Cataldi, P. et al. [46]

3.3. Anticorrosion Performance of SPU Films with Modified CNT

The water absorption of the composite free-standing film before and after modification was checked by immersing the samples in deionized water, 1 wt% HCl and 1 wt% NaOH solution for 48 h. The results are shown in Figure 8d. Compared with the literature values in Table 2, our CNT-SPU component showed very low water absorption. The water absorptions of ***CNT-SPU*** (Figure 8a) in H_2O, 1% HCl and 1% NaOH solution were 0.390, 0.380 and 0.395 wt%, respectively. Compared to the ***CNT-SPU*** with unmodified CNT, the water absorption of the modified CNT in composite SPU films (Figure 8b–e) decreased slightly, suggesting that the modification of CNT improved the water resistance and chemical solvent resistance of the material. Especially the SiO_2–TiO_2 modified composite film has the lowest water absorption in all three media. Compared with ***CNT-SPU***, it is reduced by 7.6% in the water medium and 6.3% in the chemical medium. This may be due to the addition of CNT_{MO} makes the film more compact, making it difficult for the solvent to penetrate it and not easy to expand when immersed in water. After CNT is modified by KH540 and KH560, the silane coupling agent acts as a "molecular bridge" in the elastomer, which can enhance the adsorption force of the substrate and reduce the degree of freedom of chain segments. This has a certain shielding effect on water molecules, improving the water resistance and chemical resistance of SPU films. The water resistance and chemical resistance of the CNT_{NCO}***-SPU*** films deteriorated because of the serious phase separation of the film, which is also reflected in the SEM (Figure 5e_2).

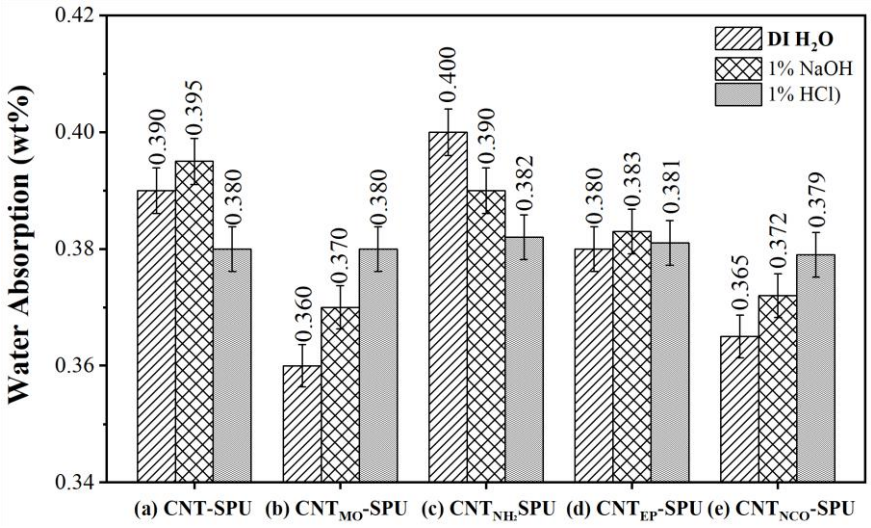
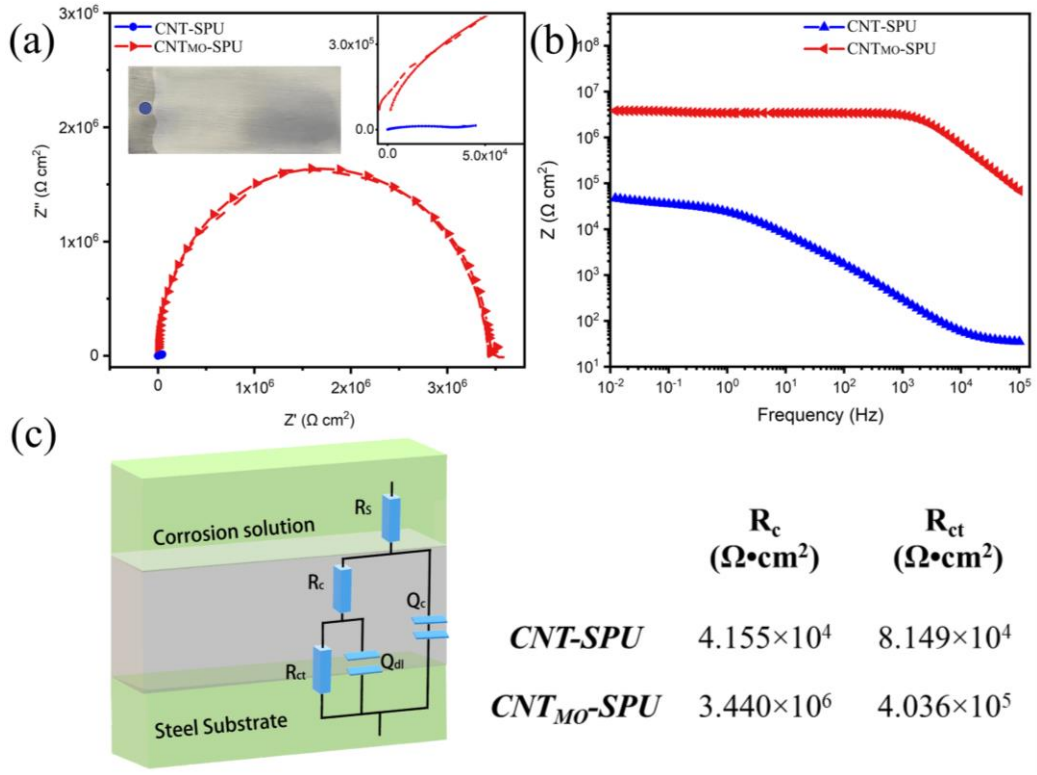


Figure 8. Water resistance of composite free-standing film before and after modification: (**a**) ***CNT-SPU***, (**b**) CNT_{MO}***-SPU***, (**c**) CNT_{NH2}***-SPU***, (**d**) CNT_{EP}***-SPU***, (**e**) CNT_{NCO}***-SPU***.

In the water and chemical resistance tests, the CNT_{MO}***-SPU*** film has the best performance, indicating that the film is dense and has good protective properties for the substrate. Therefore, to explore the corrosion resistance of CNT_{MO} filler, the same composite resin (CNT_{MO}***-SPU***) was coated on polished tinplate and further immersed in 3.5 wt% NaCl solution for 48 h to test their corrosion resistance. The Nyquist plots and Bode plots can also be used to characterize

the corrosion resistance of the ***CNT$_{MO}$-SPU* coating**, as shown in Figure 9a,b. The larger the radius in the Nyquist curve is, the larger the polarization resistance, indicating that the coating has a better corrosion resistance [19]. Moreover, in the Bode plot, the high impedance value in the low-frequency region ($|Z|_{f=0.01Hz}$) means that the coating has good corrosion resistance. The impedance radius of ***CNT$_{MO}$-SPU coating*** is much larger than that of ***CNT-SPU coating*** (Figure 9a), indicating the ***CNT$_{MO}$-SPU coating*** has a better anticorrosion ability. The EIS fitting results (summarized in Figure 9c) are based on the equivalent circuit diagram model shown in Figure 9c. The resistance coating (R_c) of ***CNT$_{MO}$-SPU coating*** (3.440×10^6 Ω•cm^2) is much larger than that of SPU-CNT (4.155×10^4 Ω•cm^2). This means the electrolyte is difficult to penetrate, so the charge transfer number (R_{ct}) of ***CNT$_{MO}$-SPU coating*** (4.036×10^5 Ω•cm^2) is also larger than that of ***CNT-SPU coating*** (8.149×10^4 Ω•cm^2). Besides, in the impedance diagram of ***CNT$_{MO}$-SPU coating***, there is only one capacitive arc, and there is no Warbury arc, indicating that the composite coating can play a better protective role when the substrate is not corroded. The Bode plots obtained from this test are shown in Figure 9b). In the Bode plot, the impedance moduli of ***CNT-SPU coating*** and ***CNT$_{MO}$-SPU coating*** are 4.72×10^4 Ω•cm^2 and 3.84×10^6 Ω•cm^2, respectively. The larger impedance mode of ***CNT$_{MO}$-SPU*** composite coating indicates that the ***CNT$_{MO}$*** can serve as an excellent barrier in the composite coating.



	R_c (Ω•cm^2)	R_{ct} (Ω•cm^2)
CNT-SPU	4.155×10^4	8.149×10^4
CNT$_{MO}$-SPU	3.440×10^6	4.036×10^5

Figure 9. Nyquist (**a**) and Bode plots (**b**) of the synthesized ***CNT-SPU*** and ***CNT$_{MO}$-SPU*** coatings after 48 h immersion in 3.5 wt% NaCl solution. The insert in (**a**) upper left corner is the photo of ***CNT$_{MO}$-SPU*** coating. The equivalent circuit diagram model of coatings is shown in (**c**), and the main parameters of EIS fitting for ***CNT-SPU*** and ***CNT$_{MO}$-SPU*** coatings are also listed in (**c**).

Figure 10 and Table 3 are the results of potentiodynamic polarization curves. Potentiodynamic polarization curves are often used to characterize the electrochemical corrosion resistance of materials, and the corrosion current density (i_{corr}) and corrosion potential (E_{corr}) can be used to compare the corrosion resistance of different materials or coatings [47–50]. Generally, the lower the i_{corr} is, the better the corrosion resistance. Compared with ***CNT-SPU coating*** (i_{corr}: 1.599×10^{-5} A/cm^2), the i_{corr} value of ***CNT$_{MO}$-SPU coating*** reduced to 9.246×10^{-9} A/cm^2. This is also consistent with the results of EIS above. The anticorrosion ability is comparable with those using epoxy resin (as listed in Table 3 for comparison),

indicating that they can serve well for metal-substrate protection. This may be because the ***CNT$_{MO}$*** added to the coating is more evenly distributed in the SPU matrix, which could effectively prevent the migration of water molecules, as sketched in Figure 10b,c. Based on the above results and analysis, the anticorrosion effect of the ***CNT$_{MO}$-SPU*** coating is mainly attributed to the ***CNT$_{MO}$*** nanoparticles in SPU coating, and the water resistance test of the coating confirmed that the ***CNT$_{MO}$-SPU*** composite coating has good barrier properties to the electrolyte. In addition, the SiO_2–TiO_2 on the surface of ***CNT$_{MO}$*** is more likely to form micro-nano structures, which increases the crosslinking degree between ***CNT$_{MO}$*** and SPU. This is beneficial for the ***CNT$_{MO}$*** filler embedding in SPU and can effectively improve the performance of the coating, as reported before [51]. Finally, as a filler, ***CNT$_{MO}$*** can block the pores of the coating and prevent the electrolyte penetration coating from corroding the metal substrate.

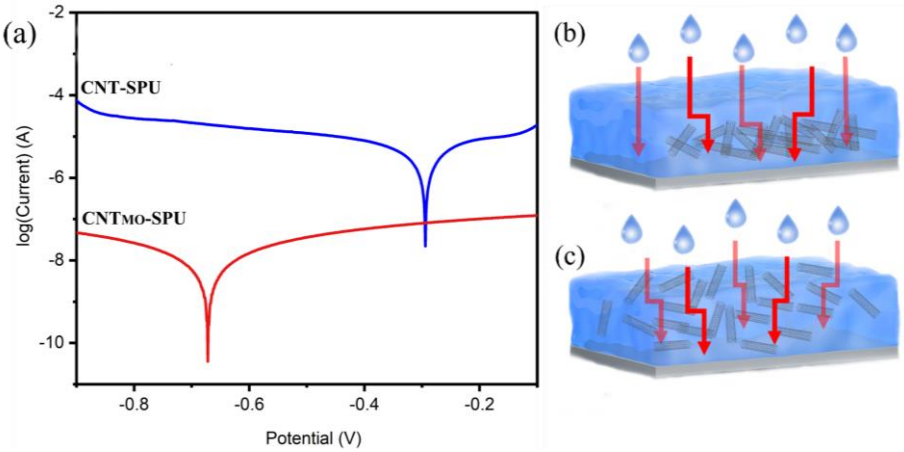


Figure 10. Potentiodynamic polarization curves (**a**), anticorrosion schematics (**b**,**c**) of ***CNT-SPU coating*** and ***CNT$_{MO}$-SPU coating***.

Table 3. Results of potentiodynamic polarization test for different coatings.

Sample	E_{corr} (V)	i_{corr} (A/cm^2)	ba (mV/decade)	−bc (mV/decade)	μ (g·m^{-2}·h^{-1})
CNT-SPU coating	–0.297	1.599×10^{-5}	3.877	2.681	1.66×10^{-1}
CNT$_{MO}$-SPU coating	–0.672	9.246×10^{-9}	5.046	4.882	9.62×10^{-5}
5% coating [52]	–0.083	1.78×10^{-8}			
H05G08EP [53]	–0.77	5.6×10^{-7}			
1 mM TTA [54]	–0.427	7.28×10^{-7}	58.6	–77.8	
CPED/epoxy resin-treated [55]	–1.27	6.0×10^{-5}			
EA+500nmSiO_2+P+Gr [50]	–0.532	7.1×10^{-9}	631	111	7.24×10^{-5}

4. Conclusions

CNT were functionalized by different approaches, and four modified CNT samples were obtained: ***CNT$_{MO}$***, ***CNT$_{NH2}$***, ***CNT$_{EP}$*** and ***CNT$_{NCO}$***. After figuring out the structures of the modified CNT samples, they were dispersed in homemade SPU resin to prepare composite coatings, and the mechanical and anticorrosion properties of the composite coating were analyzed. In the mechanical tests, the ***CNT$_{MO}$-SPU*** film exhibited the best tensile strength (3.45 MPa) and elongation at break (162%), which were better than the corresponding values of ***CNT-SPU*** (2.81 MPa, 146%). Besides, ***CNT$_{MO}$-SPU*** coating also showed the best chemical resistance and anticorrosion ability, with a low water adsorption ratio and low corrosion current density. This may be due to the micro-nano structures of SiO_2–TiO_2 modified CNT surface. The increase of surface roughness of the ***CNT$_{MO}$*** material can further improve the dispersion of the filler in the SPU resin, resulting in enhancing the mechanical and anticorrosion performance of the coating.

Author Contributions: J.Y.: conceptualization; G.H., X.L., S.W. (Shuchuan Wang) and S.W. (Shirong Wang): Investigation; G.H.: writing—original draft preparation; J.Y. and M.R: writing—review and editing; J.Y. and M.R.: supervision. All authors have read and agreed to the published version of the manuscript.

Funding: This work is financed by the Natural Science Foundation of Shanghai (No. 23ZR1425700).

Institutional Review Board Statement: Not applicable.

Informed Consent Statement: Not applicable.

Data Availability Statement: All data that support the findings of this study are included within the article.

Acknowledgments: Thanks to Runkai Wang (SUES) and Li Wang (North Paint & Coatings Industry Research and Design Institute) for scientific discussion about this work.

Conflicts of Interest: The authors declare no conflict of interest.

References

1. Ristic, I.S.; Budinski-Simendic, J.; Krakovsky, I.; Valentova, H.; Radicevic, R.; Cakic, S.; Nikolic, N. The properties of polyurethane hybrid materials based on castor oil. *Mater. Chem. Phys.* **2012**, *132*, 74–81. [CrossRef]
2. Yilgor, I.; Yilgor, E.; Wilkes, G.L. Critical parameters in designing segmented polyurethanes and their effect on morphology and properties: A comprehensive review. *Polymer* **2015**, *58*, A1–A36. [CrossRef]
3. Rostami, A.; Moosavi, M.I. High-performance thermoplastic polyurethane nanocomposites induced by hybrid application of functionalized graphene and carbon nanotubes. *J. Appl. Polym. Sci.* **2020**, *137*, 48520. [CrossRef]
4. Valuev, I.L.; Valuev, L.I.; Obydennova, I.V.; Sytov, G.A.; Vanchugova, L.V. Modified polyurethanes as a new type of thromboresistant polymers. *Polym. Sci. Ser. A* **2010**, *52*, 824–827. [CrossRef]
5. Cheng, F.; Fan, Y.; He, N.; Song, Y.; Shen, J.; Gong, Z.; Tong, X.; Yang, X. Castor oil based high transparent UV cured silicone modified polyurethane acrylate coatings with outstanding tensile strength and good chemical resistance. *Prog. Org. Coat.* **2022**, *163*, 106624. [CrossRef]
6. Galhenage, T.P.; Hoffman, D.; Silbert, S.D.; Stafslien, S.J.; Daniels, J.; Miljkovic, T.; Finlay, J.A.; Franco, S.C.; Clare, A.S.; Nedved, B.T.; et al. Fouling-release performance of silicone oil-modified siloxane-polyurethane coatings. *ACS Appl. Mater. Interfaces* **2016**, *8*, 29025–29036. [CrossRef] [PubMed]
7. Yin, C.; Okamoto, R.; Kondo, M.; Tanaka, T.; Hattori, H.; Tanaka, M.; Sato, H.; Iino, S.; Koshiro, Y. Electrospinning of block and graft type silicone modified polyurethane nanofibers. *Nanomaterials* **2019**, *9*, 34. [CrossRef]
8. Zadeh, Z.E.; Solouk, A.; Shafieian, M.; Nazarpak, M.H. Electrospun polyurethane/carbon nanotube composites with different amounts of carbon nanotubes and almost the same fiber diameter for biomedical applications. *Mater. Sci. Eng. C* **2021**, *118*, 111403. [CrossRef]
9. Alberto, M.; Iliut, M.; Pitchan, M.K.; Behnsen, J.; Vijayaraghavan, A. High-grip and hard-wearing graphene reinforced polyurethane coatings. *Compos* **2021**, *213*, 108727. [CrossRef]
10. Charpentier, P.A.; Burgess, K.; Wang, L.; Chowdhury, R.R.; Lotus, A.F.; Moula, G. Nano-TiO_2/polyurethane composites for antibacterial and self-cleaning coatings. *Nanotechnology* **2012**, *23*, 425606. [CrossRef]
11. Zou, B.; Huang, C.Z.; Wang, J.; Liu, B.Q. Effect of nano-scale TiN on the mechanical properties and microstructure of Si_3N_4 based ceramic tool materials. *Adv. Mach. Manuf. Technol. Viii* **2006**, *315–316*, 154–158. [CrossRef]
12. Guerrero-Martinez, A.; Perez-Juste, J.; Liz-Marzan, L.M. Recent progress on silica coating of nanoparticles and related nanomaterials. *Adv. Mater.* **2010**, *22*, 1182–1195. [CrossRef]
13. Gonzalez-Carrero, S.; Galian, R.E.; Perez-Prieto, J. Organometal halide perovskites: Bulk low-dimension materials and nanoparticles. *Part. Part. Syst. Char.* **2015**, *32*, 709–720. [CrossRef]
14. He, Y.; Chen, C.; Zhong, F.; Chen, H.; Qing, D. Synthesis and properties of iron oxide coated carbon nanotubes hybrid materials and their use in epoxy coatings. *Polym. Adv. Technol.* **2015**, *26*, 414–421. [CrossRef]
15. Bai, Y.; Park, I.S.; Lee, S.J.; Bae, T.S.; Watari, F.; Uo, M.; Lee, M.H. Aqueous dispersion of surfactant-modified multiwalled carbon nanotubes and their application as an antibacterial agent. *Carbon* **2011**, *49*, 3663–3671. [CrossRef]
16. Bhattacharyya, A.; Joshi, M. Functional properties of microwave-absorbent nanocomposite coatings based on thermoplastic polyurethane-based and hybrid carbon-based nanofillers. *Polym. Adv. Technol.* **2012**, *23*, 975–983. [CrossRef]
17. Wang, J.L.; Meng, L.J. Influence of carbon nano-fiber on mechanical property of PALC. *Energy Eng. Environ. Eng.* **2014**, *535*, 785–787. [CrossRef]
18. Wu, Q.; Miao, W.-S.; Zhang, Y.-D.; Gao, H.-J.; Hui, D. Mechanical properties of nanomaterials: A review. *Nanotechnology* **2020**, *9*, 259–273. [CrossRef]
19. Wang, F.; Feng, L.; Lu, M. Mechanical properties of multi-walled carbon nanotube/waterborne polyurethane conductive coatings prepared by electrostatic spraying. *Polymers* **2019**, *11*, 714. [CrossRef]

20. Zhang, C.; Vennerberg, D.; Kessler, M.R. In situ synthesis of biopolyurethane nanocomposites reinforced with modified multi-walled carbon nanotubes. *J. Appl. Polym. Sci.* **2015**, *132*, 42515. [CrossRef]
21. Sainsbury, T.; Fitzmaurice, D. Templated assembly of semiconductor and insulator nanoparticles at the surface of covalently modified multiwalled carbon nanotubes. *Chem. Mat.* **2004**, *16*, 3780–3790. [CrossRef]
22. Xiao, Y.-K.; Ji, W.-F.; Chang, K.-S.; Hsu, K.-T.; Yeh, J.-M.; Liu, W.-R. Sandwich-structured rGO/PVDF/PU multilayer coatings for anti-corrosion application. *RSC Adv.* **2017**, *7*, 33829–33836. [CrossRef]
23. He, Y.; Ming, Y.; Li, W.; Li, Y.F.; Wu, M.Q.; Song, J.Z.; Li, X.J.; Liu, H. Highly stable and flexible pressure sensors with modified multi-walled carbon nanotube/polymer composites for human monitoring. *Sensors* **2018**, *18*, 1338. [CrossRef] [PubMed]
24. Zeng, W.; Liu, F.; He, J. Physicochemical properties of Bis-GMA/TEGDMA dental resin reinforced with silanized multi-walled carbon nanotubes. *Silicon* **2019**, *11*, 1345–1353. [CrossRef]
25. Rastogi, R.; Kaushal, R.; Tripathi, S.K.; Sharma, A.L.; Kaur, I.; Bharadwaj, L.M. Comparative study of carbon nanotube dispersion using surfactants. *J. Colloid. Interf. Sci.* **2008**, *328*, 421–428. [CrossRef] [PubMed]
26. Aguiar, V.O.; Pita, V.J.R.R.; Marques, M.D.F.V. Nanocomposites of ultrahigh molar mass polyethylene and modified carbon nanotubes. *J. Appl. Polym. Sci.* **2019**, *136*, 47459. [CrossRef]
27. Meng, H.; Yan, T.; Yu, J.; Jiao, F. Super-hydrophobic and super-lipophilic functionalized graphene oxide/polyurethane sponge applied for oil/water separation. *Chin. J. Chem. Eng.* **2018**, *26*, 957–963. [CrossRef]
28. Haghdadeh, P.; Ghaffari, M.; Ramezanzadeh, B.; Bahlakeh, G.; Saeb, M.R. Polyurethane coatings reinforced with 3-(triethoxysilyl)propyl isocyanate functionalized graphene oxide nanosheets: Mechanical and anti-corrosion properties. *Prog. Org. Coat.* **2019**, *136*, 105243. [CrossRef]
29. Li, S.; Du, X.; Hou, C.; Hao, X.; Jia, J.; Guan, T.; Yi, T.; Ma, G. One-pot two-step perfluoroalkylsilane functionalization of multi-walled carbon nanotubes for polyurethane-based composites. *Compos. Sci. Technol.* **2017**, *143*, 46–55. [CrossRef]
30. Taraghi, I.; Paszkiewicz, S.; Fereidoon, A.; Szymczyk, A.; Stanik, R.; Gude, M.; Linares, A.; Ezquerra, T.A.; Piesowicz, E.; Wilpiszewska, K.; et al. Thermally and electrically conducting polycarbonate/elastomer blends combined with multiwalled carbon nanotubes. *J. Thermoplast. Compos.* **2021**, *34*, 1488–1503. [CrossRef]
31. Navidfar, A.; Sancak, A.; Yildirim, K.B.; Trabzon, L. A study on polyurethane hybrid nanocomposite foams reinforced with multiwalled carbon nanotubes and silica nanoparticles. *Polym. Plast. Technol. Eng.* **2018**, *57*, 1463–1473. [CrossRef]
32. Wang, A.; Wang, Y.; Yu, W.; Huang, Z.; Fang, Y.; Long, L.; Song, Y.; Cifuentes, M.P.; Humphrey, M.G.; Zhang, L.; et al. TiO_2-multi-walled carbon nanotube nanocomposites: Hydrothermal synthesis and temporally-dependent optical properties. *RSC Adv.* **2016**, *6*, 20120–20127. [CrossRef]
33. Ţucureanu, V.; Matei, A.; Avram, A.M. FTIR spectroscopy for carbon family study. *Crit. Rev. Anal. Chem.* **2016**, *46*, 502–520. [CrossRef] [PubMed]
34. Li, X.; Yang, J.; Wang, J.; Chang, X.; Xu, J.; Wu, Z. A stable super-amphiphilic surface created from superhydrophobic silica/epoxy coating by low-temperature plasma-treatment. *Surf. Eng.* **2021**, *37*, 1282–1289. [CrossRef]
35. Yang, J.; Zhang, J.; Zou, B.; Zhang, H.; Wang, J.; Schubert, U.; Rui, Y. Black SnO_2–TiO_2 nanocomposites with high dispersion for photocatalytic and photovoltaic applications. *ACS Appl. Nano Mater.* **2020**, *3*, 4265–4273. [CrossRef]
36. Zhang, D.; Shi, L.; Fang, J.; Li, X.; Dai, K. Preparation and modification of carbon nanotubes. *Mater. Lett* **2005**, *59*, 4044–4047. [CrossRef]
37. Deng, H.; Zhang, H. In situ synthesis and hydrothermal crystallization of nanoanatase TiO_2–SiO_2 coating on aramid fabric (HTiSiAF) for UV protection. *Microsc. Res. Tech.* **2015**, *78*, 918–925. [CrossRef]
38. Ren, C.; Qiu, W.; Zhang, H.; He, Z.; Chen, Y. Degradation of benzene on $TiO_2/SiO_2/Bi_2O_3$ photocatalysts under UV and visible light. *J. Mol. Catal. A Chem.* **2015**, *398*, 215–222. [CrossRef]
39. Zhang, M.; Lin, Z.; Huang, Q.; Zhu, Y.; Hu, H.; Chen, X. Green synthesis of submicron-sized Ti-rich MWW zeolite powders via a novel mechanochemical dry gel conversion in mixed steam environment. *Adv. Powder Technol.* **2020**, *31*, 2025–2034. [CrossRef]
40. Wang, G.; Wen, S.; Qian, S.; Wang, J.; Wang, C.; Chen, Y. Synthesis of novel nano hyperbranched polymer resin and its corrosion resistance in coatings. *Prog. Org. Coat.* **2020**, *140*, 105496. [CrossRef]
41. Qian, Y.; Dong, F.; Guo, L.; Xu, X.; Liu, H. Terpene derivative-containing silicone two-component waterborne polyurethane for coatings. *Prog. Org. Coat.* **2021**, *153*, 106137. [CrossRef]
42. Tijing, L.D.; Park, C.-H.; Kang, S.-J.; Amarjargal, A.; Kim, T.-H.; Pant, H.R.; Kim, H.J.; Lee, D.H.; Kim, C.S. Improved mechanical properties of solution-cast silicone film reinforced with electrospun polyurethane nanofiber containing carbon nanotubes. *Appl. Surf. Sci* **2013**, *264*, 453–458. [CrossRef]
43. Kurańska, M.; Aleksander, P.; Mikelis, K.; Ugis, C. Porous polyurethane composites based on bio-components. *Compos. Sci. Technol.* **2013**, *75*, 70–76. [CrossRef]
44. Zhang, X.J.; Cai, Y.Q.; Zhang, X.W.; Aziz, T.; Fan, H.; Bittencourt, C. Synthesis and characterization of eugenol-based silicone modified waterborne polyurethane with excellent properties. *J. Appl. Polym. Sci.* **2021**, *138*, 47562. [CrossRef]
45. Xu, S.; Xie, L.; Yu, X.; Xiong, Y.; Tang, H. Synthesis and characterization of phenyl polysiloxane modified polyurea/polyurethanes. *J. Polym. Sci. Part A Polym. Chem.* **2015**, *53*, 1794–1805. [CrossRef]
46. Cataldi, P.; Profaizer, M.; Bayer, I.S. Preventing water-induced mechanical deterioration of cardboard by a sequential polymer treatment. *Ind. Eng. Chem. Res.* **2019**, *58*, 6456–6465. [CrossRef]

47. Guo, L.; Jing, L.Z.; Liu, Y.; Zou, B.J.; Hua, S.C.; Zhang, J.P.; Yu, D.Y.; Wang, S.C.; Wang, S.R.; Wang, L.D.; et al. Enhanced Dispersion of Graphene in Epoxy-Acrylic Waterborne Anticorrosion Coating: Bifunctional Ligands Linking Graphene to SiO_2. *Int. J. Electrochem. Sci.* **2018**, *13*, 11867–11881. [CrossRef]
48. Zou, B.; Chang, X.; Yang, J.; Wang, S.; Xu, J.; Wang, S.; Samukawa, S.; Wang, L. Plasma treated h-BN nanoflakes as barriers to enhance anticorrosion of acrylic coating on steel. *Prog. Org. Coat.* **2019**, *133*, 139–144. [CrossRef]
49. Li, H.; Wang, J.; Yang, J.; Zhang, J.; Ding, H. Large CeO_2 nanoflakes modified by graphene as barriers in waterborne acrylic coatings and the improved anticorrosion performance. *Prog. Org. Coat.* **2020**, *143*, 105607. [CrossRef]
50. Shen, Y.F.; Yang, J.X.; Wang, S.C.; Jing, L.Z.; Zheng, H.; Du, Y.Y.; Zou, B.J.; Lei, X.Z.; Xu, J.L. Size Influences of SiO_2-graphene Barrier on the Corrosion Resistance of Epoxy-Acrylic Waterborne Coating. *Int. J. Electrochem. Sci.* **2021**, *16*, 151018. [CrossRef]
51. Hsu, Y.W.; Wu, C.C.; Wu, S.M.; Su, C.C. Synthesis and Properties of Carbon Nanotube-Grafted Silica Nanoarchitecture-Reinforced Poly (Lactic Acid). *Materials* **2017**, *10*, 829. [CrossRef] [PubMed]
52. Liao, Z.; Zhang, T.; Qiao, S.; Zhang, L. Preparation and Electrochemical Properties of Graphene/Epoxy Resin Composite Coating. *IOP Conf. Ser. Earth Environ. Sci.* **2017**, *94*, 012072. [CrossRef]
53. Xu, H.Y.; Li, B.; Han, X.; Wang, Y.; Zhang, X.R.; Komarneni, S. Synergic enhancement of the anticorrosion properties of an epoxy coating by compositing with both graphene and halloysite nanotubes. *J. Appl. Polym. Sci.* **2019**, *136*, 47562. [CrossRef]
54. Damej, M.; Hsissou, R.; Berisha, A.; Azgaou, K.; Sadiku, M.; Benmessaoud, M.; Labjar, N.; El hajjaji, S. New epoxy resin as a corrosion inhibitor for the protection of carbon steel C38 in 1M HCl. experimental and theoretical studies (DFT, MC, and MD). *J. Mol. Struct.* **2022**, *1254*, 132425. [CrossRef]
55. Ji, R.; Ma, M.; He, Y.; Liu, C.; Fang, T.; Zhang, Z.; Wang, Y.; He, Y.; Wu, J. Improved corrosion resistance of Al_2O_3 ceramic coatings on AZ31 magnesium alloy fabricated through cathode plasma electrolytic deposition combined with surface pore-sealing treatment. *Ceram. Int.* **2018**, *44*, 15192–15199. [CrossRef]

Disclaimer/Publisher's Note: The statements, opinions and data contained in all publications are solely those of the individual author(s) and contributor(s) and not of MDPI and/or the editor(s). MDPI and/or the editor(s) disclaim responsibility for any injury to people or property resulting from any ideas, methods, instructions or products referred to in the content.